Research Article

iMedPub Journals
www.imedpub.com

Nano Research & Applications
ISSN 2471-9838

2019
Vol. 5 No. 12

DOI: 10.36648/2471-9838.5.1.39

Size Separation of Gold Nanorods at the Periphery of Coffee-Stain Ring

Ahmad I*

Department of Physics, University of Peshawar, Khyber Pakhtunkhwa, Pakistan

***Corresponding author:** Ahmad I

imtiaz@uop.edu.pk

Department of Physics, University of Peshawar, Khyber Pakhtunkhwa, Pakistan.

Tel: +914712520268

Citation: Ahmad I (2019) Size Separation of Gold Nanorods at the Periphery of Coffee-Stain Ring. Nano Res Appl Vol .5 No.1:2

Abstract

Droplet drying techniques showed in many studies that nanoparticles generally self-assembles in a coffee-stain ring after complete evaporation of the solvent. Suspension comprise of various shapes and sizes in suspension dried on SiO_2 substrate at room temperature leaves behind a coffee- stain like ring. High resolution scanning electron microscope (HRSEM) images for at various locations of the coffee-stain ring display some interesting self-assembling behaviour of various shapes of the gold nanostructures. At outer-edges of the deposited ring, side-by-side assembly of nanorods showed that such assembly begins with a thin nanorod and ends with thick ones. In case of thick-thin rods and spheres with relatively dense concentration allows merely thick rods ensemble while other observed in disorder everywhere within the ring. Theoretical nano- interactions also affirms experimental results.

Keywords: Self-assembly; Gold nanorods; Coffee-stain ring; Shape-separation

Received: June 14, 2019; **Accepted:** June 25, 2019; **Published:** July 03, 2019

Introduction

Self-assembly of nanoparticles is significant for constructing materials that can be involve to recognize the collective properties of the resulting superstructures, with uses in optics, electronics, and catalysis [1-3] these applications can be a lot different from those of the building blocks [4-6]. Recently, many classes of nanoparticle superstructures have been achieved using various schemes, for instance electrostatic forces, biomolecular recognition, and entropic effects [7-16]. Over the past few years, it has been shown that combination of various shapes can immensely enhance the phase behavior of the consequent superstructures [17-21]. Even so, there exist a lot of room to practically overcome the limitations that often hinder the translation of those ideas into experimental realization. Moreover, understanding and manipulation of self-assembly of nanoentities together with shape and size separation still needs noticeable consideration.

A sessile drop including nanoentities in suspension when dried on a substrate generally form a ring like structure, known as "coffee-stain ring". Using optical microscope, it has been observed that upon evaporation of solvent, suspended particles in a droplet migrate towards the three phase contact-line, consequently develop the capillary flow mechanism that leads to the formation of ring-stain ring [22]. Evaporation driven self-assembly is vastly important for the reason that it is simple, inexpensive, and one can achieve various ranges (nano to micro) of assembled arrays.

At present, structural diversity of nanoparticles is increasing and with that curiosity is also growing, to understand their self-assembling as well as self-separation behaviour. For instance, experiments have revealed that nanorods and nanospheres can self-assemble into stripes like superstructures at the proximity of the outer edge of the coffee-stain ring. Consequently, establish phase-separate effect in suspension as well as such deposits demonstrate order to disorder transition as one move from outer to inner edge of the coffee-stain ring [23].

We show here that various sizes of gold nanorods in suspension preferentially self-organize mostly at the outer edge of the coffee-stain ring. Two different techniques are employed to observe and understand their self-assembly behaviour. First we synthesize gold nanorods that comprise of various sizes in suspension. Secondly two different aspect ratio (AR3 and AR6) nanorods are mixed in a define portion. The former showed assembly of side-by-side arrays of gold nanorods that mostly begins with a thinner rod and ends with a thicker rod located at the outer edge of the coffee-stain ring. The later however shows thick nanorods assembly while thin nanorods plus spheres mixture did not assembled. Such results are explained in terms of concentration and possible interactions at the nanoscale.

© Under License of Creative Commons Attribution 3.0 License | **This article is available in:** http://nanotechnology.imedpub.com/archive.php

Material and Methods

Materials

Cetyltrimethylammonium bromide (CTAB, Aldrich, 98%), hydrogen tetrachloroaurate ($HAuCl_4 \bullet 3H_2O$, 99.999%, Aldrich), silver nitrate ($AgNO_3$, 99%, Acros), ascorbic acid (AA, 99%, Merck), sodium borohydrate ($NaBH_4$, 99%, Aldrich), and hydrochloric acid (HCl, 37%, Merck) were all used as received without further purification. All water that was used in the synthesis was of Milli-Q quality (18.2 MΩcm), produced in a Simplicity 185 system (Millipore).

Synthesis and Deposition

One step synthesis technique was used for making of gold nanorods with various sizes. First, solution of 10 mL (0.2M) CTAB in water was placed at 30°C for at least half an hour to dissolve CTAB completely in water. Then 25 µL of $HAuCl_4$ (0.1 M) was introduce with contenous sterring followed by 27 µL (0.1 M) of AA with 200 µL (0.1 M) NaOH. Finally, 50 µL (0.01M) of $AgNO_3$ was added and left for overnight at room temperature.

We used the 2-step seed mediated protocol, as explained by Nikoobakht and El-Sayed [24] to produce gold nanorods for this study. Initially, CTAB-coated seed solution was prepared by adding 25 µL of $HAuCl_4$ (0.1 M) in 10 mL of CTAB (0.1 M). At that time, 60 µL of ice-cold $NaBH_4$ (0.1 M) was added with continuously stirring for at least 5 min. This solution was quickly turned light brown, indicating the formation of gold seeds. The resulting solution was kept at 25°C for 2 h to attain saturation of the seed formation.

For aspect ratio (AR) 3 gold nanorods, growth solution was prepared by introducing 50 µL of $HAuCl_4$ (0.1 M) in 10 mL of CTAB (0.1 M). The resulting solution was heated at 35°C for 30 min with slow stirring to dissolve CTAB and was left to cooldown to 25°C. At this temperature, 25 µL of $AgNO_3$ (0.1 M) was introduced and then followed by 70 µL of ascorbic acid (0.1 M) with mild stirring; this solution quickly turned colorless. Then, 150 µL of HCl (1 M) was added and pH of the solution was maintained at 3. Lastly, 24 µL of the seed solution was introduced into the growth solution. This solution was left uninterrupted overnight at 2 °C.

In the same way for AR6 nanorods, growth solution was prepared by adding 50 µL of $HAuCl_4$ (0.1 M) in 10 mL of CTAB (0.1 M). This solution was kept at 35°C for 30 min to completely dissolve CTAB. Then keeping the solution at 25°C, 20 µL of $AgNO_3$ (0.1 M) was introduced. At that time, 70 µL of ascorbic acid (0.1 M) was added into the growth solution which is followed by 100 µL of HCl (1 M). Lastly, 24 µL of seed solution was added into the growth solution and was left undisturbed overnight at room temperature.

All prepared suspensions were centrifuged at 15000 rpm for 10 min to take out the excess CTAB. Similarly, the same growth solution (AR3) were centrifuged again at 5600 rpm for 5 min to separate nanospheres from the nanorods. The supernatant comprising mostly nanorods was cautiously separated from the settled precipitate in the bottom of the centrifuge tube; the latter comprises of mostly spheres. These nanorod suspensions were stored in the refrigerator.

For drop-casting depositions, SiO_2 substrates were ultrasonically washed in distilled water for 10 min at room temperature. Followed by the further cleaning of the substrates, which were rinsed twice with distilled water and dried in a nitrogen flow. Suspensions droplets (5 µL) of each solution were placed on the clean SiO_2 substrate and allowed to evaporate at room temperature. Nearly within 3 hours the solvent is completely disappeared, leaving a coffee-stain ring on the surface.

Characterization

Ultraviolet-visible (UV-VIS) spectroscopy was performed using two different setups: (a) a Varian Cary 300 Scan spectrometer (for measurement of spectra in the range of 200-900 nm) and (a) an Ocean Optics HR2000+ spectrometer run using the SpectraSuite software package in combination with Mikropack UV-VIS light source (model DH-2000-BAL) (for the measurement up to wavelengths of 1100 nm). We employed standard semimicro UV cuvettes with outer dimensions of 12.5 mm × 12.5 mm × 45 mm for the optical investigation; the optical path through the solution amounts to 10 mm. Such cuvettes can hold up to 1.5 mL of solution, allowing investigation of limited volumes of solution. UV-VIS spectrums of prepared gold nanorods are shown in **Figure 1** From the analysis of transverse and longitudinal peak positions in the UV–vis curves, we deduce that the gold nanorods concentration for black curve amounts to approximately 1.2×10^{10} cm^{-3}, likewise for blue curve the densities of nanorods amounts to 4.7×10^{11} cm^{-3}. Also, for UV-VIS spectra represented by red curve contains gold nanorods which amounts to approximately 2.1×10^{10} cm^{-3} whereas for the same red curve nanospheres number densities equal to approximately 2.2×10^{10} cm^{-3}.

High-resolution scanning electron microscopy (HRSEM; on a Merlin Zeiss 1550 system) was performed for imaging of our samples; typical accelerating voltages in the range 0.1-30 kV are accessible. All images in this work were taken at 2 kV.

Results

Suspension droplet after evaporation of the solvent typically leaves behind a coffee-stain like deposits within a fix ring. SEM images at two different locations within the coffee-stain ring are shown in the **Figure 2**. Red arrows in both **Figures 2A and 2B** indicating the direction of motion of the three phase contact line

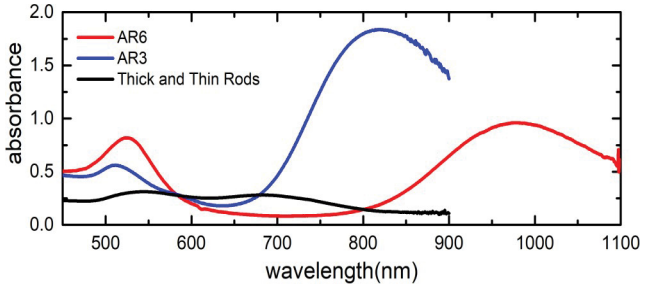

Figure 1 UV-VIS spectroscopic plots of synthesized gold nanorods. One step synthesis of nanorods spectrum is displayed by black curve. Red curve represent AR6 and blue curve shows AR3 gold nanorods.

during drying. At extreme right of the SEM images, gold nanorods assembled nicely in side-by-side fashion. Close examination of the several images reveal that such parallel arrangements with respect to the droplet contact line display analogous trend of side-by- side assembly everywhere within the ring. Likewise, these initial gold nanorod deposits at the outer proximity of the contact line by and large self-assembled according to their sizes. There, typically deposition originates from thin rod and ends with a relatively thicker rod and such deposits are merely comprises of monolayer arrays of nanorods. Furthermore, as one moves inward from the outer edge of the coffee-stain ring, side-by-side assembled building blocks display no prefer orientation as well as no signs of size selectively and separation. Moreover, assembly of nanorods away from the outer edge appears to be no more monolayer rather grows into a dense multilayered superstructure as depicted in **Figure 2A**. SEM image at different location as depicted in **Figure 2B**, shows completely different behaviour away from the outer edge. Likewise, small nanorods together with some sphere like particles deposit there in disordered, showing no specific trend.

Close examination of SEM images largely demonstrate similar trend at the proximity of the outer edge of coffee-stain ring as displayed in **Figure 3**. SEM images in **Figures 3A and 3B** display large overview of the initial assemble arrays of gold nanorods demonstrating side-by-side assembly of 10-20 nanorods in considerably analogous manner. Such deposits are further enlarged in **Figures 3C and 3D**, which shows self-organizations of nanorods merely at the proximity of the coffee-stain ring. Once again, demonstrating essentially the similar behaviour of self-assembly which begins with thin rods and finishes with the relatively thicker ones.

To statistically interpret such formations at the proximity of the outer end of the coffee- stain ring, several SEM images are examined for this purpose. Histograms were plotted for nearly 200 rods within the side-by-side arrays, width of each nanorod within the deposited array was measured. For instance, width of first nanorod that deposit on the surface was measured then second and so on up to the tenth nanorod in each assembled array. Width distribution of first five nanorods at the outer edge of the coffee-stain ring are shown in **Figure 4A** whereas from rod number 6th to 10th within the similar arrays of gold nanorods are shown in **Figure 4B**. The inset in **Figure 4** is showing the mean value of the width of nanorod at the particular location within the assembled array in each histogram.

Next thick and thin gold nanorod mixture was used to further understand such the size separation effect. For this purpose gold nanorods of AR3 that contain thick nanorods (width~12 nm) and AR6 gold nanorods which comprises of thin rods with average diameter of 8 nm (width ~ 8 nm). Also, AR6 suspensions contains significant amount of spheres with the gold nanorods. The ration of mixing was kept 60% of AR6 and 40% of AR3 gold nanorods. SEM results for such mixture is displayed at various locations of the coffee-stain ring in **Figure 5**. Overview of two different locations at the coffee-stain ring are shown in **Figures 5A and 5B**, where red arrows pointing towards the motion of contact line

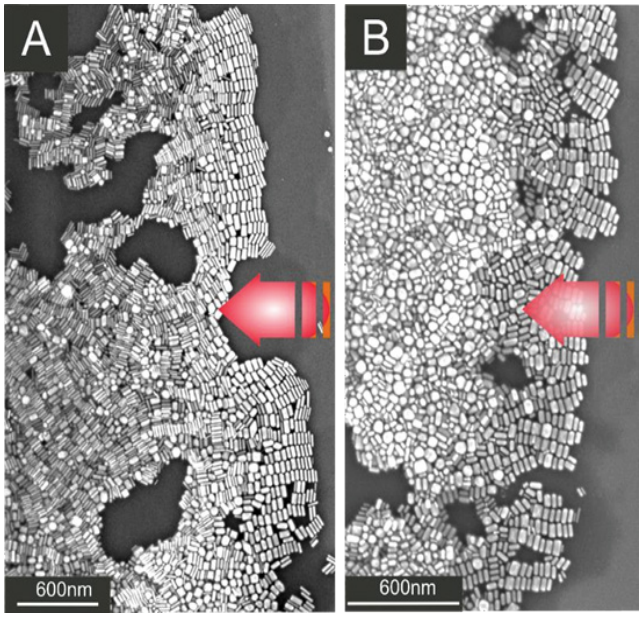

Figure 2 SEM image of gold nanorod comprises of various sizes deposit in a coffee-stain ring. (A, B) outer-edge of the stain deposits at the two different locations within the ring, red arrows pointing towards the direction of drying.

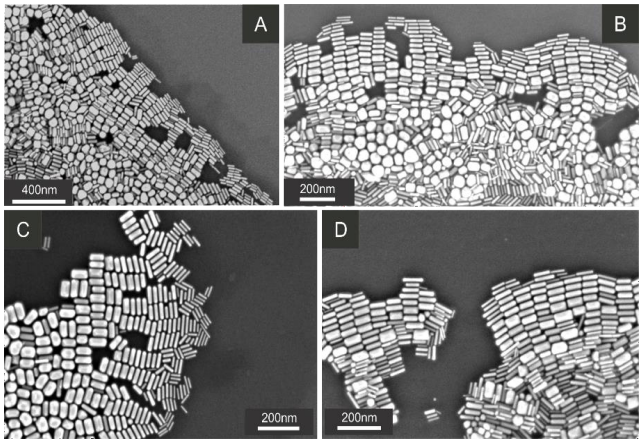

Figure 3 SEM image of gold nanorod comprises of various sizes deposit in a coffee-stain ring. (A, B) outer-edge of the stain deposits at the two different locations within the ring, red arrows pointing towards the direction of drying.

during drying. Both SEM images are displaying the similar trend, where nanorods self-assembled in side-by-side fashion and their long axis are oriented parallel to the three phase contact line. In most cases within such SEM images gold nanorod arrays are self-assembled in the analogous way up to the length of 6-7µm as depicted in **Figures 5A and 5B**. However, within the similar images away from the outer edge, no ordered arrangements are observed. A closer view of such deposits over these locations shows that these assembled arrays of gold nanorods are formed merely by thick nanorods whereas thin-rods and spheres like nanoparticles are set up in complete disorder as shown in

© Under License of Creative Commons Attribution 3.0 License

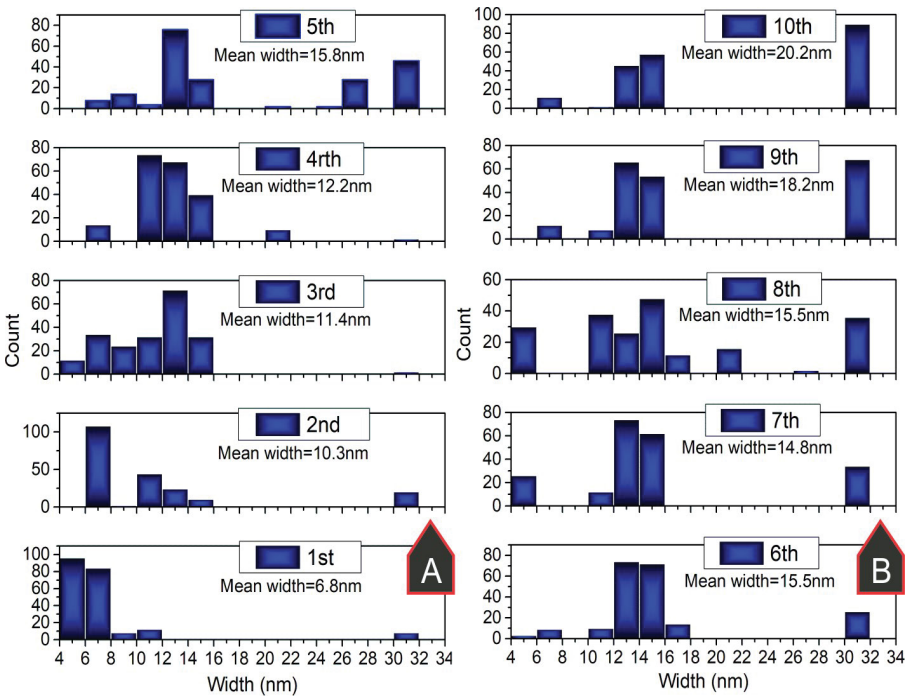

Figure 4 Histogram of gold nanorod deposits at the outer-edge of the coffee-stain ring. (A) Starting from the outer edge: counts for 1st, 2nd, 3rd, 4th and 5th nanorods. (B) Similarly counts for 6th, 7th, 8th, 9th and 10th nanorod. The inset shows rod position and means width of gold nanorods.

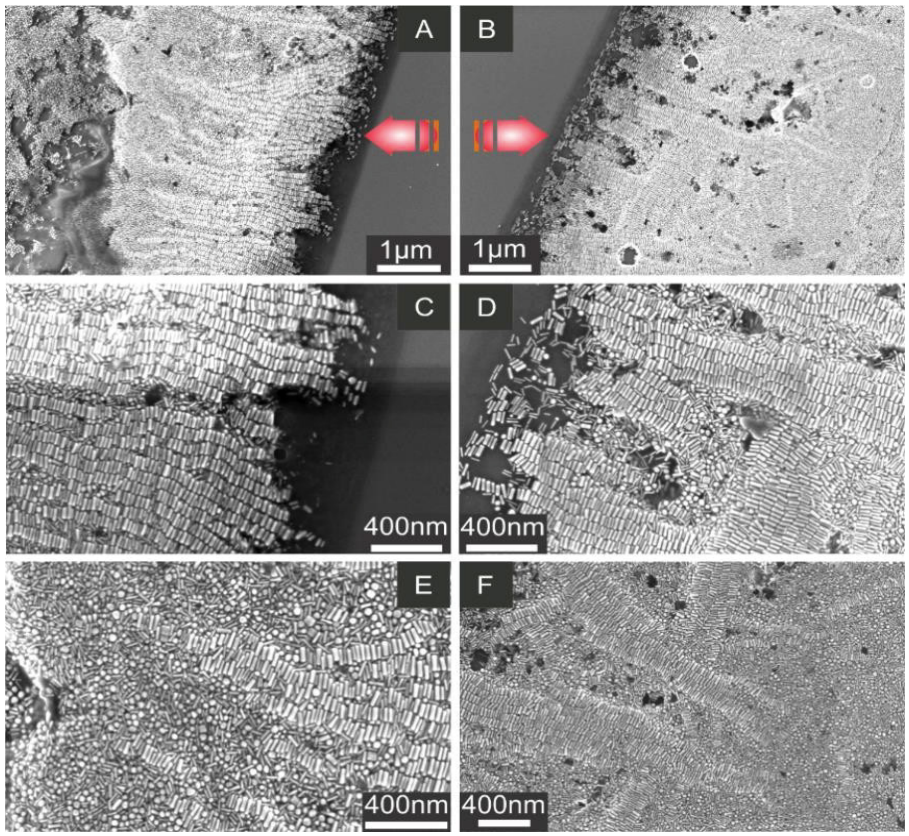

Figure 5 (A, B) SEM images of gold nanorod mixture contains AR3 and AR6 rods at two different positions of the coffee-stain ring. Red arrows show the direction of drying. (C, D) Zoom in on the outer edge of the coffee- stain ring in A and B respectively. (E, F) Inner regions away from the outer edge of the coffee-stain.

Figures 5C and 5D. Furthermore, thin-rod and sphere mixture found mostly away from the outer-edge. However, investigation of several SEM images reveal that thin-rods and spheres laying underneath the self-assembled arrays of thick nanorods. Inner deposits in the coffee-stain ring are displayed in **Figures 5E and 5F**, where tail of side-by-side assembled thick-rods is shown in the vicinity of the disordered thin-rods and spheres.

Discussion

The formation of self-assembly as a result of droplet drying mechanism essentially establishes convictive flow towards the three-phase contact line within the droplet owing to relatively faster evaporation rate at the droplet ends than the center. Consequently, such convective flow migrate nearly all suspended entities towards the three-phase contact line as shown in **Figure 6A**. In the end after complete evaporation of the aqueous phase, suspension droplet leaves behind a ring like structure on the surface that merely comprises of nanoparticle arrays as depicted in **Figure 6B**. Now there are two major possibilities for the nanoparticles in suspension: (i) Relatively diluted suspension, suggests more free space among particles which allow them to gather and then assemble at the close vicinity of the contact line, and in case of (ii) High density nanoparticles assembles away from the contact line and in the end settles in various orientations near the edge. Thus in suspension, concentration and size variations of nanoparticles seem to have pronounced effect on self-assembly mechanism.

For instance, in case of thick and thin nanorods, pronounced size separation observed specially at the proximity of the outer edge of the coffee-stain like ring. As recorded by the SEM images, it was observed that commonly side-by-side assembly of gold nanorods begins with the thinner particles and usually ends with the thicker ones. Suggesting that within a suspension droplet these nanoparticles migrate towards the three-phase contact line, where thin nanorods generally in the beginning of the assembled arrays showing that convective flow first brings thinner rods towards the edge followed by thicker particles owing to the different flow rate. Thin nanorods due to their small sizes flow relatively faster than the thick nanorods. As side-by-side array progresses towards the inner region of the coffee-stain ring, width of nanorods increases almost linearly as shown in **Figure 7**.

Theoretically combination of attractive and repulsive interactions like depletion, Van der Waals, and electrostatic forces described elsewhere [25] between two nanorods are employed on such system to understand the formation of their self-assembled arrays. For instance, if length of a gold nanorod is 30 nm with a diameter amounts to 10 nm, for these parameters the theoretical plots in **Figure 8** shows that energetically favorable assembly of two gold nanorods is side-by-side (SS) arrangement whereas least favorable or energetically less probable position for the two nanorods in suspension is end-to-end (EE) arrangement. The depth of potential well in case of end-to-end arrangement is nearly 1 kT as depicted in **Figure 8A** while depth of such potential well deepens further (4 kT) in case of side-by-side assembly. Therefore, such side-by-side arrangement not only experimentally more feasible but also agrees theoretically.

Interestingly for relatively high concentration of thick-thin gold nanorods with significant amount of spheres-like particles, only thick rods were found assembled side-by-side parallel with the contact line whereas thin nanorods and spheres were observed everywhere on the surface in chaos. It seems that thin nanorods and spheres in suspension act like depletants that facilitate thick nanorods to assemble side-by-side. Moreover, most of these thin-rods and spheres were observed away from the outer edge of the coffee-stain ring. Justifying our claim that these particles act like depletants and deposit away from the assemble arrays of thick nanorods.

Theoretically, the interaction energy is more attractive for thick nanorods (diameter = 16 nm) while in case of thin nanorods such energy is significantly low as shown in **Figure 9**. Thin nanorods the depth of potential well is around 4kT while in case of thick nanorods depth of potential well increases and having value around 6.5kT. So two thick nanorods in suspension attract one another more strongly than the thin nanorods. As a result, probability of thick nanorods to assemble in suspension increases as witnessed in SEM images displayed above.

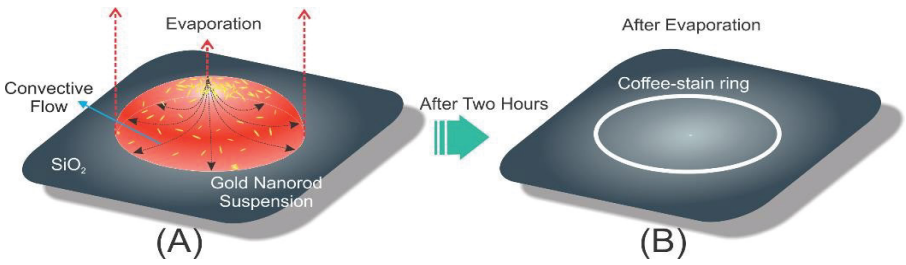

Figure 6 (A) Scheme of gold nanorod suspension placed in the form of a droplet on SiO_2 substrate, red dashed arrows are showing different evaporation rate while black dashed curved arrows within the droplet is the representation of convictive flow towards the three-phase contact line. (B) After complete evaporation of aqueous phase, nearly all suspended entities deposit in a coffee-stain like ring.

© Under License of Creative Commons Attribution 3.0 License

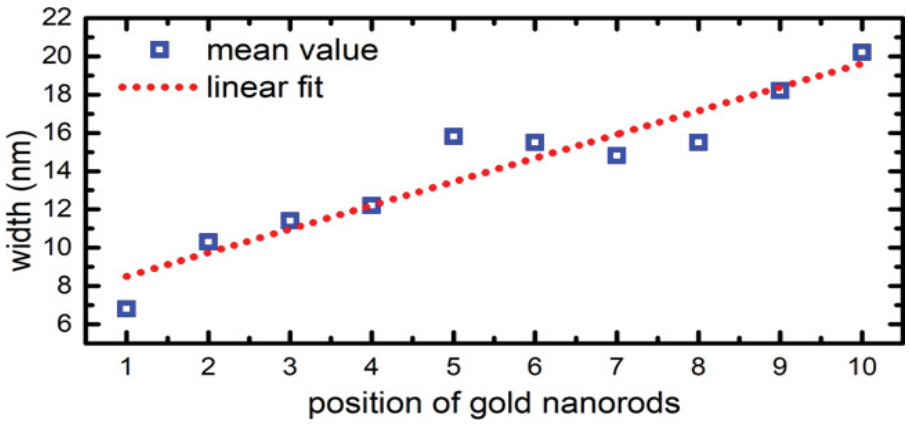

Figure 7 Blue squares indicate mean values of the width of gold nanorods with respect to their position within the side-by-side self-assemble array while red dotted line represents the linear fit.

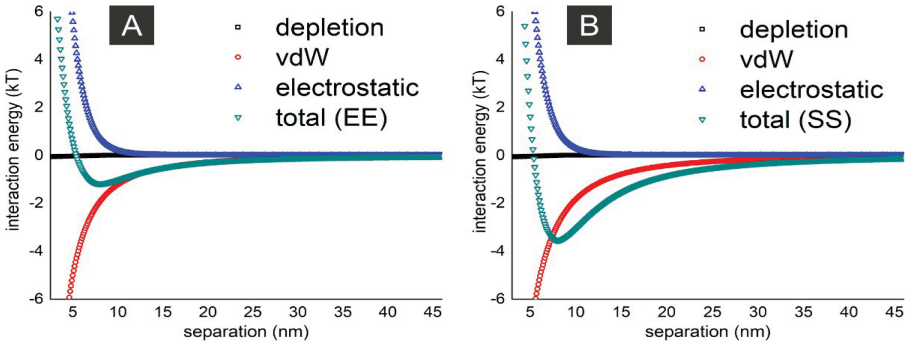

Figure 8 Depletion, Van der Waals, electrostatic, and total interactions are plotted for (A) end-to-end arrangement of two nanorods and (B) side-by-side gold nanorods.

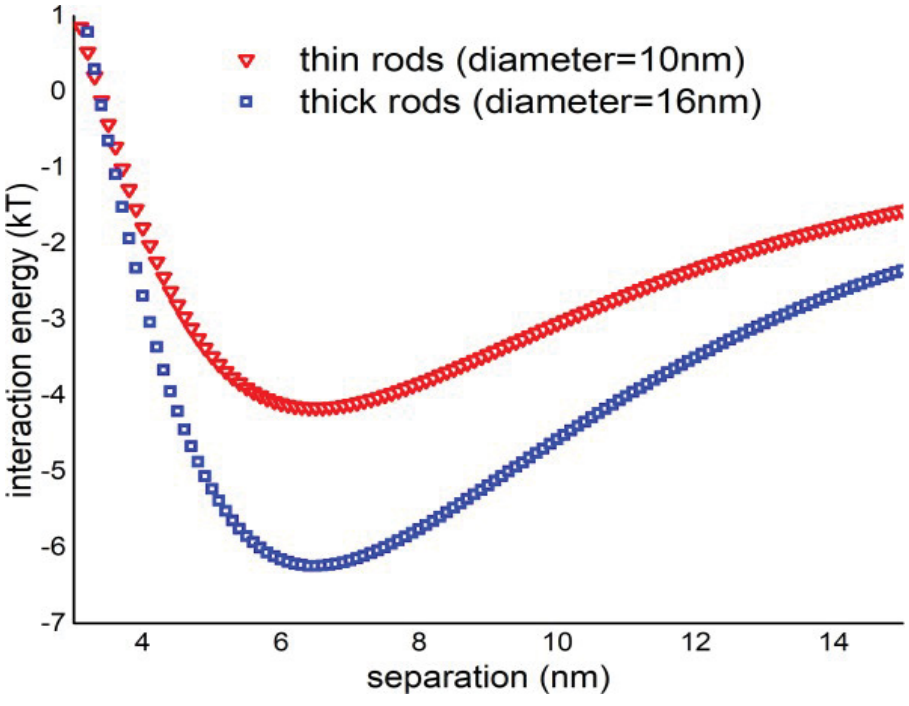

Figure 9 Interaction energy curves for two gold nanorods of diameters 10 nm and 16 nm.

This article is available in: http://nanotechnology.imedpub.com/archive.php

It is difficult for nanoparticles to get assemble in a dense environment that comprises of three different geometries like thin rods, thick rods, and spheres with collective concentration in suspension amounts to 8.1×10^{31} cm^{-3}. On the basis of SEM images, it is evident that in a dense environment strongest interaction survives and as a result assembles with its own kind. However, thin-rods and spheres in a chaotic environment could not possibly find free space to ensemble.

Conclusion

Self-assembly of two different systems are investigated. As prepared polydisperse gold nanorods assembled side-by-side near the outer edge of the contact line with specially size distribution. Such assembly generally begins from thin rod and ends with relatively thick rods. Analysis of several SEM images showed that as the assembled array progresses towards the inner region of the coffee- stain ring, the diameter of gold nanorods increases. On the other hand, mixture of various shapes and sizes owing to their dense concentration in suspension merely facilitate thick nanorods while thin-rods and spheres were observed in disorder mostly found away from the outer edge of the coffee-stain ring. In theory, energetically most feasible assembly for the two nanorods in suspension is side-by-side arrangement and for the thick nanorods such interactions are more effective than thin nanorods in suspension.

References

1 Sun S, Murray CB, Weller D, Folks L, Moser A (2000) Mono-disperse FePt nanoparticles and ferromagnetic FePt nanocrystal superlattices. Science 287: 1989-19992.

2 Rockstuhl C, Lederer F, Etrich C, Pertsch T, Scharf T (2007) Design of an artificial three-dimensional composite metamaterial with magnetic resonances in the visible range of the electromagnetic spectrum. Phys Rev Lett 99: 017401.

3 Mann S (2009) Self-assembly and transformation of hybrid nano-objects and nanostructures under equilibrium and non-equilibrium conditions. Nat Mater 8: 781.

4 Glotzer SC, Solomon MJ (2007) Anisotropy of building blocks and their assembly into complex structures. Nat Mater 6: 557.

5 Tao A, Sinsermsuksakul P, Yang P (2007) Tunable Plasmonic Lattices of Silver Nanocrystals. Nat. Nanotechnol 2: 435-440.

6 Stebe KJ, Lewandowski E, Ghosh M (2009) Materials Science. Oriented Assembly of Metamaterials. Science 325: 159-160.

7 Nykypanchuk D, Maye MM, Van Der Lelie D, Gang O (2008) DNA-guided crystallization of colloidal nanoparticles. Nature 451: 549.

8 Maye MM, Nykypanchuk D, Cuisinier M, Van Der Lelie D, Gang O (2009) Stepwise surface encoding for high-throughput assembly of nanoclusters. Nat Mater 8: 388.

9 Xiong H, Van der Lelie D, Gang O (2009) Phase behavior of nanoparticles assembled by DNA linkers. Phys Rev Lett 102: 015504.

10 Park SY, Lytton-Jean AK, Lee B, Weigand S, Schatz GC, et al. (2008) DNA-programmable nanoparticle crystallization. Nature 451: 553.

11 Macfarlane RJ, Lee B, Jones MR, Harris N, Schatz GC, et al. (2011) Nanoparticle superlattice engineering with DNA. Science 334: 204-208.

12 Kostiainen MA, Hiekkataipale P, Laiho A, Lemieux V, Seitsonen J, et al. (2013) Electrostatic assembly of binary nanoparticle superlattices using protein cages. Nat Nanotechnol 8: 52-56.

13 Zhao Y, Thorkelsson K, Mastroianni AJ, Schilling T, Luther JM, et al. (2009) Small-molecule-directed nanoparticle assembly towards stimuli-responsive nanocomposites. Nat Mater 8: 979-985.

14 Tang Z, Zhang Z, Wang Y, Glotzer SC, Kotov NA (2006) Self-assembly of CdTe nanocrystals into free-floating sheets. Science 314: 274-278.

15 Leunissen ME, Christova CG, Hynninen AP, Royall CP, Campbell AI, et al. (2005) Ionic colloidal crystals of oppositely charged particles. Nature 437: 235-240.

16 Shevchenko EV, Talapin DV, Kotov NA, O'Brien S, Murray CB (2006) Structural diversity in binary nanoparticle superlattices. Nature 439: 55-59.

17 Damasceno PF, Engel M, Glotzer SC (2012) Predictive self-assembly of polyhedra into complex structures. Science 337: 453-457.

18 Dussi S, Dijkstra M (2016) Entropy-driven formation of chiral nematic phases by computer simulations. Nat. Commun 7: 11175.

19 Reinhardt A, Frenkel D (2016) DNA brick self-assembly with an off-lattice potential. Soft Matter 12: 6253-6260.

20 Zanjani MB, Jenkins IC, Crocker JC, Sinno T (2016) Colloidal cluster assembly into ordered superstructures via engineered directional binding. ACS nano 10: 11280-11289.

21 Zhang J, Luijten E, Granick S (2015) Toward Design Rules of Directional Janus Colloidal Assembly. Annu Rev Phys Chem 66: 581−600.

22 Deegan RD, Bakajin O, Dupont TF, Huber G, Nagel SR, et al. (1997) Capillary flow as the cause of ring stains from dried liquid drops. Nature 389: 827−829.

23 Ahmad I, Zandvliet HJ, Kooij ES (2014) Shape-induced separation of nanospheres and aligned nanorods. Langmuir 30: 7953−7961.

24 Nikoobakht B, Wang ZL, El-Sayed MA (2000) Self-assembly of gold nanorods. J Phys Chem 104: 8635-8640.

25 Bishop KJ, Wilmer CE, Soh S, Grzybowski BA (2009) Nanoscale forces and their uses in self-assembly. Small 5: 1600-1630.

© Under License of Creative Commons Attribution 3.0 License